Received: 15 August 2018 | Accepted: 16 November 2018

DOI: 10.1111/jvim.15392

Journal of Veterinary Internal Medicine Open Access

ACVIM American College of Veterinary Internal Medicine

STANDARD ARTICLE

The use of diffusion tractography to characterize a corpus callosum malformation in a dog

Philippa J. Johnson[1] | **Erica F. Barry**[1] | **Wen-Ming Luh**[2] | **Emma Davies**[1]

[1]Department of Clinical Sciences, College of Veterinary Medicine Cornell University, Ithaca, New York

[2]Cornell Magnetic Resonance Imaging Facility, College of Human Ecology, Cornell University, Ithaca, New York

Correspondence
Philippa J. Johnson, Department of Clinical Sciences, College of Veterinary Medicine, Cornell University, Ithaca, New York 14853, USA.
Email: pjj43@cornell.edu

Introduction: The pathogenesis of corpus callosum malformations (CCM) is not well defined in the dog because of inherent limitations of structural magnetic resonance imaging (MRI) to evaluate the white matter. We used the advanced neuroimaging technique of tractography to virtually dissect the white matter projections in a dog with a CCM and in a normal control dog.

Methods: A 9-month-old male Coonhound that had a previous structural MRI diagnosis of CCM and a normal control dog underwent anesthesia and 3-Tesla MRI. Diffusion-tensor imaging and 3D T1-weighted and 2D T2-weighted sequences were acquired. Diffusion data were processed before tensor reconstruction and fiber tracking. Virtual dissections were performed to dissect out the major white matter projections in each dog.

Results: In the dog with CCM, the corpus callosum exhibited interhemispheric crossing fibers at the level of the splenium and formed longitudinal callosal fasciculi (Probst bundles). In addition, the fornix was small and the cingula enlarged and exhibited increased dorsal connectivity relative to the normal control.

Conclusions and Clinical Importance: We used tractography to describe a white matter malformation in a dog. The results suggest that, embryologically, formed axons fail to cross midline and instead create Probst bundles.

KEYWORDS

canine, diffusion tensor, dog, magnetic resonance imaging, MRI, white matter malformation

1 | INTRODUCTION

Corpus callosum (CC) abnormalities are a cause of adipsia and hypodipsia, leading to life-threatening hypernatremia, and long-term neurological problems in the dog.[1] This condition is associated with eventual euthanasia in approximately one-third of reported cases.[1–4] The histopathological and structural magnetic resonance imaging (MRI) features of this condition have been described in the dog but because of the inherent limitations associated with use of these techniques to document white matter structure, the underlying pathophysiology and exact malformations present in these cases still are conjectural.[1–4]

Abbreviations: AV3V, anteroventral third ventricle wall; CC, corpus callosum; CCM, corpus callosum malformation; CR, corona radiata; FOF, fronto-occipital fasiculus; LCFs, longitudinal callosal fascicles or Probst Bundles; LF, longitudinal fasiculus; MRI, magnetic resonance imaging; ROI, regions of interest; TE, echo time; TR, repetition time.

The pathogenesis and morphology of corpus callosum malformations (CCM) are well described in the human medical literature. Two types have been identified: 1 in which axons are formed, but fail to cross the midline because of the absence of the massa commissuralis within the commissural plate, running instead in a rostro-caudal direction as longitudinal callosal fascicles (LCFs), also termed Probst bundles, and another in which axons or their parent cell bodies fail to form in the cerebral cortex and LCFs (Probst bundles) are not present.[5–7] Being able to identify the exact white matter malformation present and whether LCFs are formed therefore is important for understanding which pathophysiological pathway is the cause for the malformation in an individual case. In vivo diagnosis is limited with standard structural MRI because of its inherent inability to resolve specific white matter tracts, but more recently the advanced technique of fiber tractography has been applied to the evaluation of white matter in humans with CCM.[8] This technique uses diffusion

tensor imaging to virtually reconstruct and delineate white matter fiber tracts in 3-dimensional (3D) space.[9] This technique has allowed researchers and clinicians to document white matter malformations in vivo and in greater anatomical detail than previously possible. In relation to callosal malformations, it has identified the presence or absence of Probst's bundles and documented a variety of other associated white matter abnormalities.[8,10,11]

Tractography has been used to document white matter projections in the normal canine brain and specifically to segment and delineate the CC, but this technique has not yet been applied in the evaluation of white matter malformations.[12–14] To date in the dog, CCM has only been diagnosed using standard structural MRI sequences, limiting our ability to determine the exact malformations present.[1] We used fiber tractography to document complex white matter malformations associated with a CCM in a dog. In doing so, we obtained new insight into the morphology of this condition and describe the technique of fiber tractography as a clinical tool in the evaluation of white matter malformations.

2 | MATERIALS AND METHODS

This study had approval from Cornell University's Institutional Animal Care and Use Committee.

2.1 | The CCM dog

A 9-month-old male intact Bluetick Coonhound that had a previous diagnosis of CCM was recruited for the study. On initial presentation, at 4 months of age, the dog had exhibited lethargy, dehydration, severe hypernatremia (>180 mmol/L), oculonasal discharge, hyperkeratosis of the nose, and neurological signs of a rapid vertical head tremor that was not intention-based, wide pendular head movement, and a conjugate horizontal jerk nystagmus with a fast phase to the right. Structural MRI performed using a 1.5-tesla system (Toshiba Vantage Atlas) confirmed partial CC agenesis with lack of the rostrum, genu, and body. Hospitalization and controlled IV fluid therapy stabilized the hypernatremia and the dog became clinically stable after supplementation of its food with water. On representation for repeat MRI evaluation, the owner described that, since discharge, the dog had persistent adipsia, but in other respects it has been normal. The CCM dog was described as being smaller than its littermate and learned certain tasks, such as climbing stairs, at a later age. Behaviorally, circling to the right and left and pacing were noted during periods of excitement. On neurological examination, the dog had normal mentation, posture, and gait. Postural reactions, spinal reflexes, and somatic sensation were normal. On cranial nerve evaluation, a similar type of nystagmus as observed on initial examination was identified. On physical examination no other abnormalities were detected. Serum biochemistry testing identified persistent moderate hypernatremia (sodium concentration of 163 mmol/L).

2.2 | Normal control dog

A neurologically normal 4-year-old female spayed Beagle was recruited from a research population as a comparative control. This dog had no history or clinical signs of neurological disease. It had a similar mesaticephalic head conformation as that of the CCM dog.

2.3 | Magnetic resonance imaging

Both dogs underwent general anesthesia and MRI using a General Electric Discovery MR750 3-Tesla unit (60 cm bore diameter), operating at 50 mT/m amplitude and 200 T/m/s slew rate. The dogs were placed in dorsal recumbency with their heads centered in a 16-channel medium flex radio-frequency coil (NeoCoil, LLC, Pewaukee, Wisconsin). Diffusion-tensor images were acquired in the transverse plane (repetition time [TR] = 7000 ms, echo time [TE] = 89.6 ms, flip angle = 90°, spatial resolution = 1.5 mm^3, in-plane field of view = 135 × 135 mm, matrix size = 90 × 90, slice thickness = 1.5 mm) with 60 gradient directions and a single unweighted diffusion image. The *b* value was set to 800 s/mm^2. A high resolution T1-weighted 3D inversion-recovery fast-spoiled gradient echo sequence (Bravo) was performed in each subject with the following parameters: isotropic voxels = 0.5 mm^3, TE = 3.6 ms, TR = 8.4 ms, interval = 450 ms, excitations = 3, and flip angle = 12°. Two-dimensional transverse and sagittal T2-weighted sequences were obtained for structural evaluation with the following parameters: TR = 4380 ms (transverse) 7565 ms (sagittal), TE = 94 ms, slice thickness = 2.6 mm, matrix = 512 × 512, excitations = 1, and flip angle = 111°.

2.4 | Data processing

Diffusion data were skull-stripped and corrected for noise, phase distortion, eddy current distortion, and motion using the functional MRI of the brain software library[15] and MRTrix[16] software packages. Diffusion Toolkit and TrackVis software[17] were used for tensor reconstruction and fiber tracking by a deterministic method using fiber assignment by continuous tracking. High-resolution T1-weighted 3D data were skull stripped, registered to standard space, and utilized as a 3D model for the tractography dissections.

2.5 | Structural imaging evaluation

The structural T1 and T2-weighted images of the CCM dog was evaluated in relation to the previous 1.5-Tesla MRI examination and compared to that of the normal dog.

2.6 | White matter dissections

Dissections were performed on both subjects by using the open source online software TrackVis.[17] In each data set, seed regions of interest (ROIs) were placed to dissect out the major white matter projections within each hemisphere, and included association (cingulum, longitudinal fasciculus [LF], and fronto-occipital fasciculus [FOF]), projection (corona radiata [CR]), and commissural (CC) tract groups. Placement of seed ROIs was performed in accordance with that documented in the human medical literature and any visibly spurious or artifactual tracts were removed.[18] A complete description of seed ROI placement is available in the Supporting Information. Once dissections were complete, the morphology of the tracts was evaluated both in 3D space and in 2D, after overlying the tracts on high-resolution

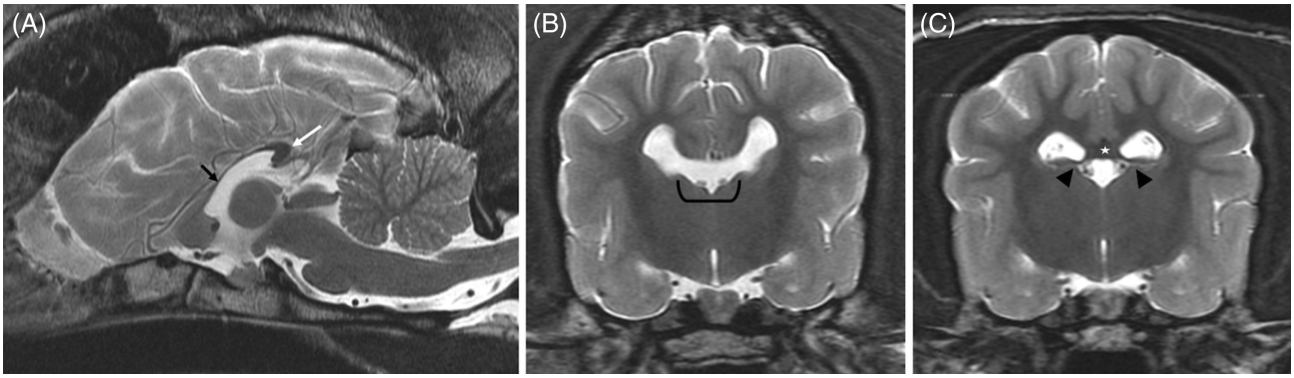

FIGURE 1 A, Midline sagittal T2-weighted image of the corpus callosum malformation (CCM) subject demonstrating the splenium (white arrow) which is the only visible portion of the corpus callosum and hypoplastic fornix (black arrow). B, Transverse mid-brain T2-weigthed image of the CCM subject demonstrating the lack of the dorsal wall of the 3rd ventricle and connection between the 3rd and lateral ventricles (black bracket). C, Transverse mid-brain T2-weighted image of the control subject demonstrating the visible corpus callosum (white star) and separation of the ventricular structures (black arrow heads)

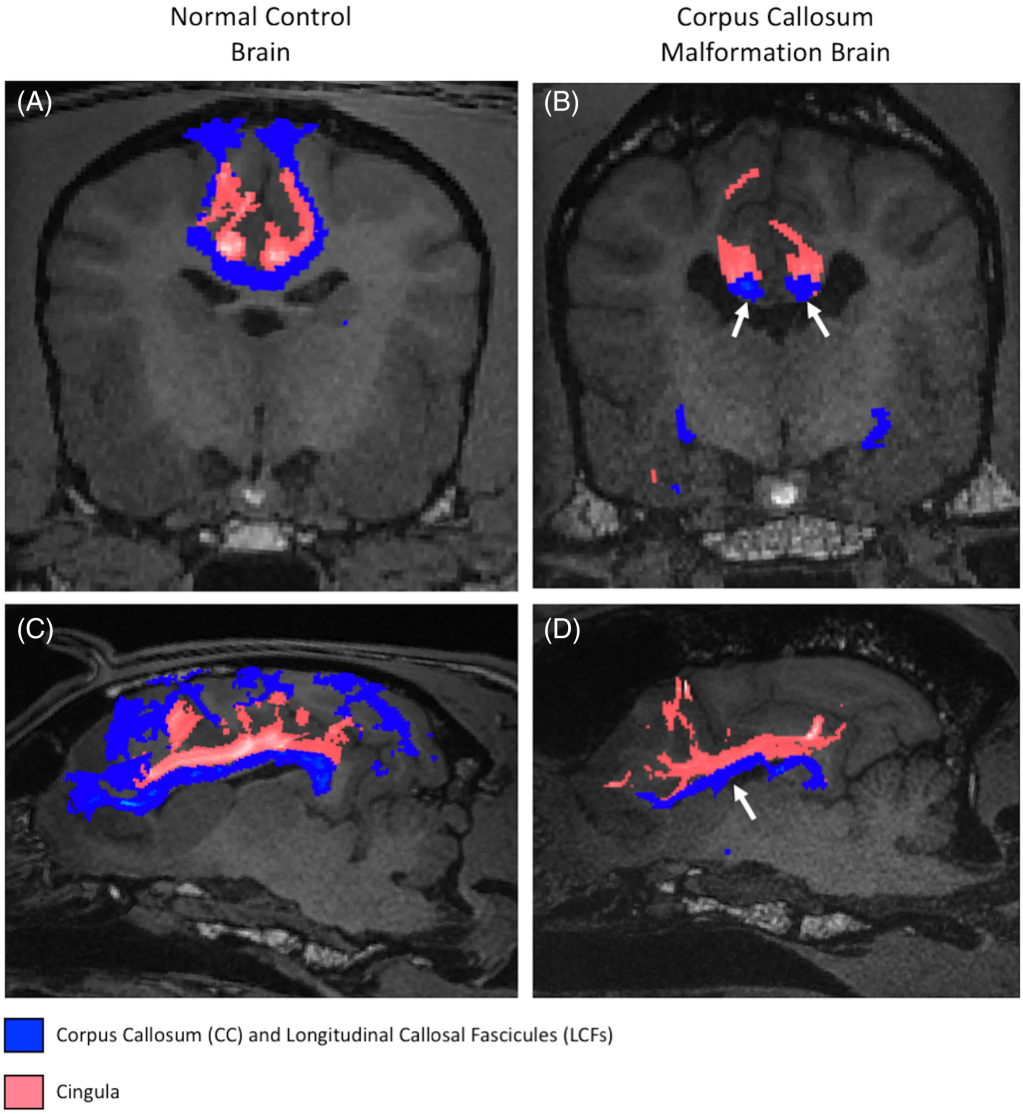

FIGURE 2 Transverse (A and B) and parasagittal (C and D) high-resolution T1-weighted 3-dimensional images with overlain dissected corpus callosum (CC) and cingula projections. The normal morphology of the CC (blue) in relation to the cingula (pink) is demonstrated in the normal control brain (A and C). The enlarged cingula and malformed CC with associated longitudinal callosal fascicules (Probst bundles) (white arrows) are demonstrated in the CC malformation brain (B and D)

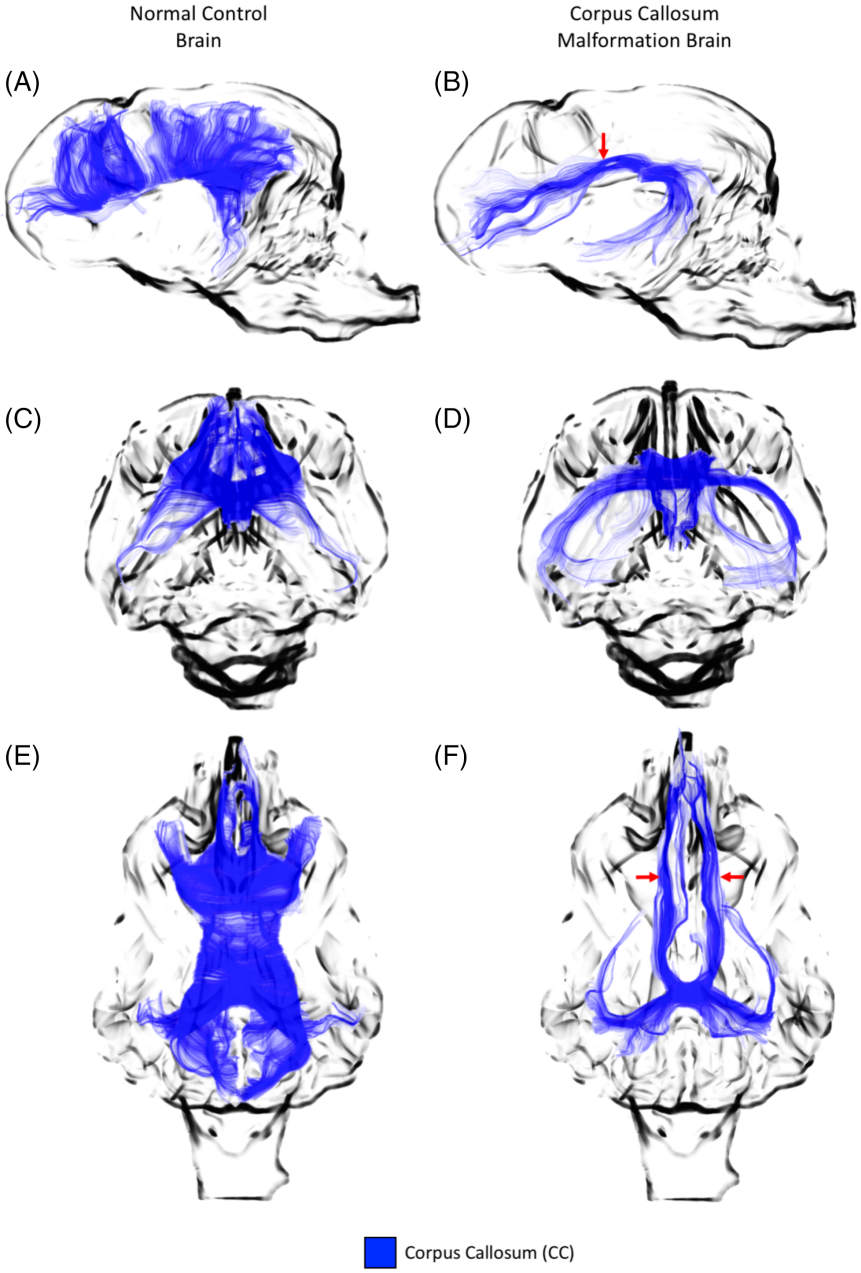

FIGURE 3 Three-dimensional images of the corpus callosum (CC) (blue) in lateral (A and B), rostro-caudal (C and D), and dorsoventral views (E and F). The normal control images (A, C, and E) demonstrate the normal morphology of the CC. The CC malformation images (B, D, and F) demonstrate the malformed structure observed in our subject. White matter axons are shown to cross at the level of the splenium only and more rostrally form rostro-caudally orientated longitudinal callosal fascicles (Probst bundles) (red arrows)

T1-weighted structural images. The white matter malformations were described in relation to the normal control dog. To gain more objective assessment of tract size, the numbers of tracts present within the projection and within the whole brain were recorded and a tract-to-whole brain ratio was calculated for each tract.

3 | RESULTS

On standard T1 and T2-weighted structural imaging of the CCM dog, only the splenium was visible within the CC. This visible remnant was small and the rostrum, genu, and body were absent. The fornix was visible, but it was small in size and the dorsal wall of the third ventricle was absent, resulting in connection with the lateral ventricles (Figure 1). These structural changes were similar to those observed on the 1.5-Tesla examination obtained on initial presentation.

On evaluation of the tractography dissections, the CCM dog had multiple white matter malformations when compared to the normal control dog. The CC had interhemispheric crossing fibers only at the level of the splenium with complete absence of crossing rostral to this region. After crossing the splenium, fibers extended both laterally into each temporal lobe and rostrally toward the frontal lobes in the form of 2 LCFs. Dorsal projections were not associated with this tract (Figures 2 and 3). The size of the CC was smaller than that observed in the normal dog

TABLE 1 The number of tracts and ratio of each tract to the whole brain for the right (R) cingulum, left (L) cingulum, right longitudinal fasciculus (R LF), left longitudinal fasciculus (L LF), right fronto-occipital fasciculus (R FOF), left fronto-occipital fasciculus (L FOF), right corona radiata (R CR), left corona radiata (L CR), fornix, and corpus callosum (CC) for each subject

	Corpus callosum malformation		Control	
	Tract number	Ratio to whole brain	Tract number	Ratio to whole brain
Whole brain	24514	NA	27014	NA
R Cingulum	7394	0.302	2525	0.093
L Cingulum	6564	0.268	2628	0.097
R LF	481	0.020	520	0.019
L LF	323	0.013	406	0.015
R FOF	1787	0.073	2027	0.075
L FOF	4201	0.171	1799	0.067
R CR	8375	0.342	6205	0.230
L CR	8649	0.353	5234	0.194
Fornix	119	0.005	3565	0.132
CC	4184	0.171	18770	0.695

(Table 1). Additional abnormalities were detected in other medially located tracts. Both cingula were larger than those observed in the normal dog and provided the majority of dorsal projections extending into the medial temporal, parietal, and occipital regions. Additionally, the fornix was markedly smaller than that observed in the normal dog (Figure 4; Table 1). The more lateral tracts within the brain also showed some mild differences. The CR in the normal dog had fibers that projected into the occipital and parietal lobes only, whereas in the CCM dog the CR was larger bilaterally and had additional fibers that extended into the frontal region (Figure 5; Table 1). The FOF and the LF both had similar sizes, shapes, locations, and connectivity in both dogs (Figure 5; Table 1).

4 | DISCUSSION

We used tractography to document a white matter malformation in the brain of a dog. This technique provided a unique method to characterize the exact location of the major white matter pathways in the brain of a dog with CCM, allowing us to accurately identify alterations in the CC and see the relationship of this malformation to other white matter tracts.

Identification of the exact white matter malformation present is important for our understanding of the underlying embryological pathophysiology of this condition. The 2 types of CCM described include 1 in which axons are formed, but fail to cross midline because of the absence of the massa commissuralis within the commissural plate, running instead in a rostro-caudal direction as LCFs, also termed Probst bundles, and another in which axons or their parent cell bodies fail to form in the cerebral cortex and LCFs (Probst bundles) are not present.[5,6] The identification of LCFs allows discrimination between these 2 types of malformations. The diagnosis of LCFs on structural sequences has been described in humans, with these aberrant white matter tracts appearing as a longitudinal widening within the medial hemispheric wall. In previous reports in dogs, this widening was not reported. Therefore, LCFs were presumed absent, and the latter pathophysiological explanation has been historically accepted.[1,4] In our dog, this widening was not identified on the structural sequences, but tractography did detect rostro-caudally orientated white matter tracts within the medial hemispheric wall, confirming the presence of LCFs (see Figures 2 and 3). The fact that we identified Probst bundles therefore broadens our understanding of the pathophysiology of this malformation and suggests that in our CCM dog, the malformation present was caused by an inability of axons to cross midline, rather than a failure of axonal formation.

The white matter malformations we identified were most marked in the midline region, with not only the CC being affected but also the cingulum, fornix, and CR. The cingula were larger and exhibited more extensive dorsal connectivity in the CCM dog, presumably in an attempt to compensate for the lack of dorsal connectivity exhibited by the CC. The fornix was markedly small in size, which may be because of the fact that the Probst bundles run in a similar fashion to the body of the fornix and could provide some of the connectivity for the hippocampus.

The most clinically relevant neurological sign in our CCM dog was adipsia. Adipsia is the most common clinical presentation associated with this condition in dogs, being reported in 12 of 15 animals in 1 case series.[1] The thirst response is mediated by multiple midline central neurological structures. Cellular dehydration is detected by osmoreceptors in the hypothalamus and also in the organum vasculosum of the lamina terminalis, subfornical organ, and median preoptic nucleus, which lie more dorsally within the anteroventral third ventricle wall (AV3V region).[19] The efferent neural pathways that project from these regions to generate a thirst response are relatively unknown, but positron emission tomographic studies have suggested that anterior and posterior portions of the cingulate cortex play a role.[20]

Historically, the adipsia observed in this condition has been suggested to occur secondary to hypothalamic malformation,[21] but a more recent publication has suggested otherwise.[1] In our CCM dog, tractography identified the most important abnormalities within the rostral portion of the CC, fornix, and cingula, which are closely associated with the AV3V region and cingulate cortex. These findings are consistent with those previously described in adipsic dogs with CCM in which partial CC agenesis consistently involved the rostral portion of the CC (rostrum, genu, and rostral body).[1] In humans with CCM, adipsia is a very rare clinical feature, and therefore by comparing the morphology of the condition in both species we may find clues about why adipsia is observed in affected dogs. One of the major morphological differences between affected humans and dogs is that when partial agenesis is present in humans it almost always involves the posterior portion of the CC (posterior body and splenium)[5] and interestingly, in the 2 case reports in humans describing adipsia secondary to CCM, the partial CC agenesis present was anterior, similar to that observed in affected adipsic dogs.[21,22] Because the rostral aspect of the CC lies in very close association with the AV3V region and the rostral cingulate cortex, these findings suggest that these more dorsal regions are important in the pathogenesis of the adipsia observed in

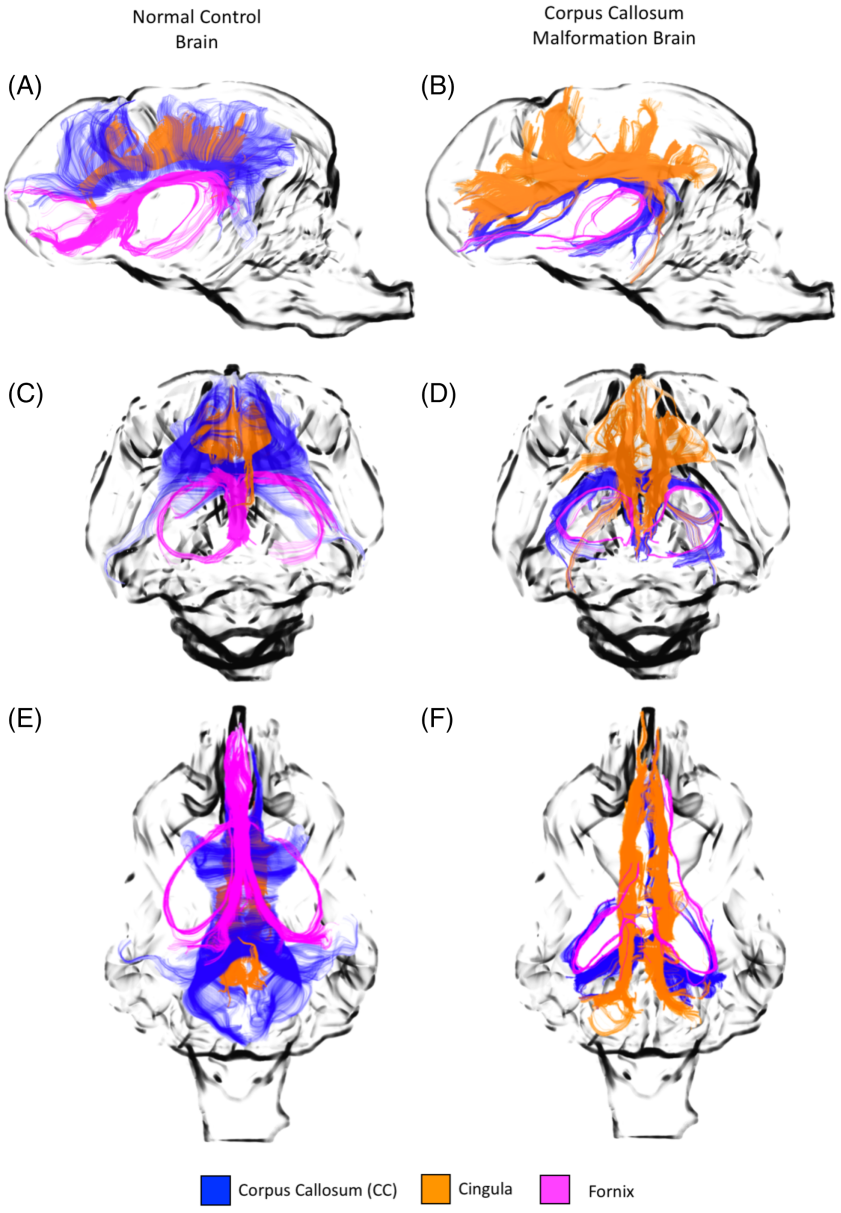

FIGURE 4 Three-dimensional images of the corpus callosum (CC) (blue), cingula (orange) and fornix (pink) in lateral (A and B), rostro-caudal (C and D), and dorsoventral views (E and F). These images demonstrate the relationship of these 3 projections in the normal control (A, C, and E) and corpus callosum malformation (CCM) brain (B, D, and F). In the CCM brain the cingula are enlarged and form the only dorsal projections extending into the medial aspect of the frontal, parietal, and occipital lobes. The fornix is small in size and the CC forms rostro-caudal projections similar to the fornix in the normal control brain

dogs with CCM. Further anatomic studies in a larger number of dogs would be required to confirm this hypothesis.

One limitation of our study is that the 9-month-old CCM subject was not compared to an age-matched control. Studies evaluating the maturing canine brain have found that, although white matter diffusivity parameters are altered at 9 months when compared to a mature brain,[23] the structure of the white matter is fully formed at this stage.[24] For this reason, although an age-matched control would have been ideal, we believe the age difference was unlikely to have substantially impacted our findings.

Ours is the first study to utilize tractography to document a CC white matter malformation in the dog. It has allowed us to dissect out multiple different projection pathways and gain greater insight into the exact malformations present. Our findings identified a different pathogenesis for the condition than previously described.[1] In our dog, we confirmed the presence of LCFs (Probst bundles), a feature of this condition previously thought not to be present in the dog.[1] This finding indicates that in our dog, this condition occurred when formed axons failed to cross midline, rather than the previously suggested failure of axonal formation.[1] Tractography also identified alterations in multiple other white matter projections, including the cingula and fornix, suggesting that the adipsia observed in our dog may be secondary to a breakdown in the thirst pathway at the AV3V or cingulate cortex level, rather than the hypothalamus, as has been suggested in the human medical literature.[21] This exploratory study only documents findings from a single CCM dog and control and therefore further studies

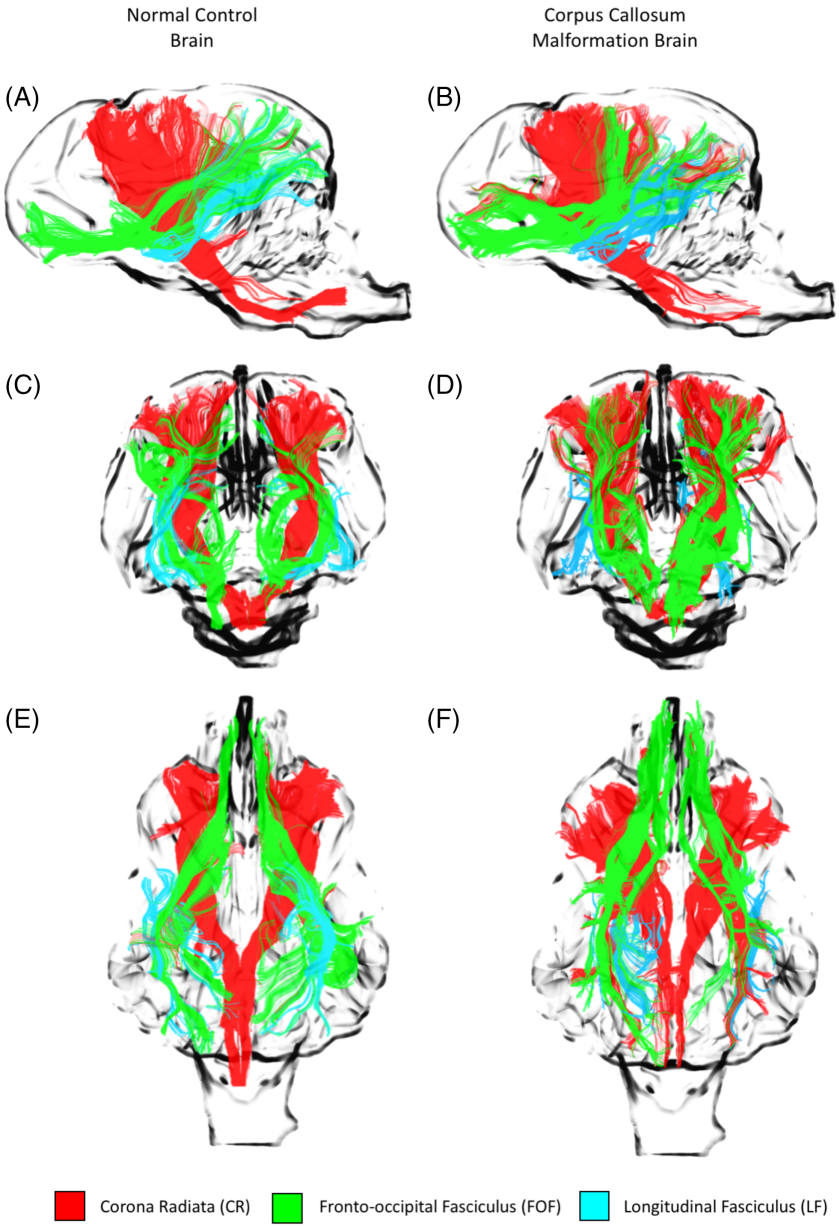

FIGURE 5 Three-dimensional images of the more lateral projections of the corona radiata (CR) (red), fronto-occipital fasciculus (FOF) (green), and longitudinal fasciculus (LF) (blue) in lateral (A and B), rostro-caudal (C and D), and dorsoventral views (E and F). These projections are similar between subjects, however the CR exhibits more connectivity to the frontal region, than is observed in the normal control subject

evaluating tractography in a larger number of dogs is required to completely characterize the malformations present in this condition.

ACKNOWLEDGMENTS

The authors thank Roy Proper for his technical expertise, Carol Fredrick and Erin Berthelson for their coordination, and Nora Mathews for her anesthetic contribution.

CONFLICT OF INTEREST DECLARATION

Authors declare no conflict of interest.

OFF-LABEL ANTIMICROBIAL DECLARATION

Authors declare no off-label use of antimicrobials.

INSTITUTIONAL ANIMAL CARE AND USE COMMITTEE (IACUC) OR OTHER APPROVAL DECLARATION

This study was approved by Cornell University's IACUC in compliance with the US National Research Council's guide for the care and use of laboratory animals, the US public health Service's policy on humane care and use of laboratory animals and guide for the care and use of live vertebrate animals in research and teaching. IACUC numbers 2015-0115 and 2016-0021.

HUMAN ETHICS APPROVAL DECLARATION

Authors declare human ethics approval was not needed for this study.

ORCID

Philippa J. Johnson https://orcid.org/0000-0002-4558-0745

REFERENCES

1. Goncalvez R, Volk H, Smith PM, et al. Corpus callosal abnormalities in dogs. *J Vet Intern Med*. 2014;28:1275-1279.
2. Sullivan SA, Harmon BG, Purinton PT, Greene CE, Glerum LE. Lobar holoprosencephaly in a Miniature Schnauzer with hypodipsic hypernatremia. *J Am Vet Med Assoc*. 2003;223(12):1783-1787.
3. Shimokawa Miyama T, Iwamoto E, Umeki S, Nakaichi M, Okuda MMT. Magnetic resonance imaging and clinical findings in a miniature Schnauzer with hypodipsic hypernatremia. *J Vet Med Sci*. 2009;71(10):1387-1391.
4. Jeffery N, Watson P. Brain malformations associated with primary adipsia identified using magnetic resonance imaging. *Vet Rec*. 2003;152(14):436-438.
5. Sztriha L. Spectrum of corpus callosum agenesis. *Pediatr Neurol*. 2005;32(2):94-101.
6. Rakic P, Yakovlev PI. Development of the corpus callosum and cavum septi in man. *J Comp Neurol*. 1968;132(1):45-72.
7. Probst M. Über den Bau des vollständig balkenlosen Groβhirns. *Arch Psychiatr*. 1901;34(3):709-786.
8. Benezit AB, Hertz-Pannier L, Dehaene-Lambertz G, et al. Organising white matter in a brain without corpus callosum fibres. *Cortex*. 2015;63:155-171.
9. Le Bihan D, Johansen-Berg H. Diffusion MRI at 25: exploring brain tissue structure and function. *Neuroimage*. 2012;61:324-341.
10. Tovar-Moll F, Moll J, De Oliveira-Souza R, Bramati I, Andreiuolo PA, Lent R. Neuroplasticity in human callosal dysgenesis: a diffusion tensor imaging study. *Cereb Cortex*. 2007;17(3):531-541.
11. Lee SK, Mori S, Kim DJ, Kim SY, Kim SY, Kim DI. Diffusion tensor MR imaging visualizes the altered hemispheric fiber connection in callosal dysgenesis. *Am J Neuroradiol*. 2004;25(1):25-28.
12. Jacqmot O, Van Thielen B, Michotte A, et al. Comparison of several white matter tracts in feline and canine brain by using Magnetic Resonance Diffusion Tensor Imaging. *Anat Rec*. 2017;1289(1):1-49.
13. Pierce TT, Calabrese E, White LE, Chen SD, Platt SR, Provenzale JM. Segmentation of the canine corpus callosum using diffusion-tensor imaging tractography. *Am J Roentgenol*. 2014;202(1):19-26.
14. Anaya García MS, Hernández Anaya JS, Marrufo Meléndez O, Velázquez Ramírez JL, Palacios Aguiar R. In vivo study of cerebral white matter in the dog using diffusion tensor tractography. *Vet Radiol Ultrasound*. 2015;56(2):188-195.
15. Smith SM, Jenkinson M, Woolrich MW, et al. Advances in functional and structural MR image analysis and implementation as FSL. *Neuroimage*. 2004;23:S208-S219.
16. Tournier J-D, Calamante F, Connelly A. MRtrix: diffusion tractography in crossing fiber regions. *Int J Imaging Syst Technol*. 2012;22(1):53-66.
17. Wang R, Benner T, Sorensen AG, Wedeen VJ. Diffusion toolkit : a software package for diffusion imaging data processing and tractography. *Proc Intl Soc Mag Reson Med*. 2007;15:3720.
18. Catani M, Howard RJ, Pajevic S, Jones DK. Virtual in vivo interactive dissection of white matter fasciculi in the human brain. *Neuroimage*. 2002;17(1):77-94.
19. McKinley MJ, Johnson AK. The physiological regulation of thirst and fluid intake. *Phys Ther*. 2004;19(1):1-6.
20. Denton D, Shade R, Zamarippa F, et al. Neuroimaging of genesis and satiation of thirst and an interoceptor-driven theory of origins of primary consciousness. *Proc Natl Acad Sci U S A*. 1999;96(9):5304-5309.
21. Komatsu H, Miyake H, Kakita S, Ikuta H. Hypoplasia of the corpus callosum associated with adipsic hypernatremia and hypothalamic hypogonadotropinism: a case report and review of the literature. *Pediatr Int*. 2001;43:683-687.
22. Kim BG, Kim KY, Park YJ, et al. A case of Adipsic hypernatremia associated with anomalous corpus callosum in adult with mental retardation. *Endocrinol Metab*. 2012;27(3):232.
23. Wu YC, Field AS, Duncan ID, et al. High *b*-value and diffusion tensor imaging in a canine model of dysmyelination and brain maturation. *Neuroimage*. 2011;58(3):829-837.
24. Gross B, Garcia-tapia D, Riedesel E, Ellinwood NM, Jens K. Normal canine brain maturation at magnetic resonance imaging. *Vet Radiol Ultrasound*. 2011;51(4):361-373.

SUPPORTING INFORMATION

Additional supporting information may be found online in the Supporting Information section at the end of the article.

How to cite this article: Johnson PJ, Barry EF, Luh W-M, Davies E. The use of diffusion tractography to characterize a corpus callosum malformation in a dog. *J Vet Intern Med*. 2019;33:743–750. https://doi.org/10.1111/jvim.15392